IEEE Access
Multidisciplinary ⋮ Rapid Review ⋮ Open Access Journal

Received 10 May 2023, accepted 23 May 2023, date of publication 30 May 2023, date of current version 7 June 2023.

Digital Object Identifier 10.1109/ACCESS.2023.3281366

RESEARCH ARTICLE

High-Dimensional Uncertainty Quantification in Electrical Impedance Tomography Forward Problem Based on Deep Neural Network

YINGGE ZHAO[1,2], LINGYUE WANG[2], YING LI[2,3], RENJIE HE[4], AND CHONGLEI MA[3]

[1]School of Intelligent Medical Engineering, Sanquan College, Xinxiang Medical University, Xinxiang, Henan 453000, China
[2]Hebei Key Laboratory of Bioelectromagnetic, School of Health Sciences and Biomedical Engineering, Hebei University of Technology, Tianjin 300130, China
[3]State Key Laboratory of Reliable and Intelligence of Electrical Equipment, Hebei University of Technology, Tianjin 300130, China
[4]Department of Radiation Oncology, MD Anderson Cancer Center, Houston, Texas 77030, USA

Corresponding author: Ying Li (yli@hebut.edu.cn)

This work was supported in part by the Natural Science Foundation of Hebei Province under Grant E2015202050; in part by the Key Science and Technology Project of Henan Province under Grant 222102210147; and in part by the Outstanding Young Teachers Program of Sanquan College, Xinxiang Medical University.

ABSTRACT In electrical impedance tomography (EIT), the uncertainty of conductivity distribution may cause the uncertainty in the forward calculation and further affect the inverse problem. In this paper, an improved univariate dimension reduction method based on deep neural network (DNN-UDR) is proposed for the high-dimensional uncertainty quantification in EIT forward problem. Firstly, DNN is studied to build a substitute model for EIT forward problem in order to solve the high-dimensional problem. Three normalized circular finite element models are established with random uniform conductivity distribution. Then UDR is used to analyze and quantify the uncertainty in the simulation with the form of probability. Compared with Monte Carlo simulation (MCS), the probability distribution of voltage is fitted, and the quantification indicators such as mean, variance, variation coefficient and covariance, are also consistent. On the other hand, with the increase of parameter dimensions, DNN-UDR accelerates the computations obviously. This indicates that DNN-UDR is effective and has high structural stability, accurate prediction results and high computational efficiency.

INDEX TERMS Electrical impedance tomography, high-dimensional uncertainty quantification, Monte Carlo simulation, substitute model.

I. INTRODUCTION

Electrical impedance tomography (EIT) aims at estimating the impedance distribution in the object from the potentials measured on the surface with appropriate configurations of the injected current patterns. It is a non-invasive monitoring technology, which is widely used in medical imaging, fluid mechanics, environmental science, nuclear power and other fields [1], [2], [3], [4], [5]. In biomedical EIT imaging problems, the impedance distribution in human tissue is usually assumed as deterministic values, but in fact it is affected by temperature, frequency, physiological state and so on [6], [7], [8], [9]. The uncertainty of the impedance distribution may cause the uncertainty of forward problem calculation and further affect the accuracy of the inverse problem. Tang et al. studied the correlation between skull structure and conductivity changes, and believed that the uncertainty of skull conductivity and thickness should be incorporated into the head model during the modeling process [10]. Suksawang et al. investigated the effect of uncertainty in excitation frequency and activation area volume on scalp voltage response [11]. The uncertainty influence on EIT results has attracted the attention of researchers in the world. Therefore, the uncertainty analysis

The associate editor coordinating the review of this manuscript and approving it for publication was Zhongyi Guo.

of impedance is an important task to optimize the design of EIT [12].

For a long time, mathematical modeling, numerical simulations and experiments are key to understanding and advancing the development of science and technology and form the backbone of predictive science. Mathematical modeling is an effective tool for numerical simulation of complex phenomena in the real world. The prediction results of model are not always reliable. Only the real-time and accurate simulation process of EIT is of practical value. Therefore, in order to judge the credibility of the prediction results, and give a high uncertainty to the error prediction results of the model so we need to model the uncertainty.

Uncertainty quantification (UQ) is to study the inherent and inevitable random uncertainty of the system in the modeling process, and then reduce the influence of the variability of the model parameters on the simulation results by the probability analysis methods [13], [14], [15]. UQ is a combination of probability theory and statistics with the real world, which implements the science of quantifying, characterizing, tracking and managing uncertainty in computational and real world systems. In the process of research, firstly, the uncertainty are modeled, secondly, the output results are analyzed by statistical methods to grasp the influence of uncertainty factors on the results, and finally the uncertainty method is evaluated [16], [17], [18], [19]. The popular probabilistic uncertainty quantification methods include Monte Carlo simulation (MCS) [20], [21], polynomial chaos expansion (PCE) [22], [23], random collocation method and other random polynomial expansions method [24], [25], [26]. As a sample-based repeated computation, MCS has high precision and low requirements on the type and scale of the research objects, but it is time consuming. It is generally applied as an experimental benchmark to judge the effectiveness of other methods [27]. PCE is an efficient method based on the polynomial expansion, which describes uncertain input variables with analytic formula. The analytic formula is composed of a weighted linear combination of a set of orthogonal polynomial basis functions with proper coefficients obtained using the least squares regression or stochastic Galerkin approach. With the increase of the variables, the analytic formula becomes complicated and the coefficient is difficult to solve. The stochastic model solution of the system becomes a limitation of polynomial expansion method, and the dimensionality reduction method significantly alleviates this limitation [28], [29]. The univariate dimension reduction (UDR) method can reduce the computational complexity of the model by transforming the high-dimensional function integration problem into multiple one-dimensional function integrals and has shown great advantages in solving the high-dimensional problems and no strong interaction between variables [30], [31], [32], [33]. So, it is expected to be applied in the study of EIT with high dimensional parameters.

UQ in EIT describes the degree to which the scalp voltage affected by the conductivity of each element. In EIT, the internal medium parameters of the target are complicate, the uncertainty of the model increases with the increase of the discrete element segmentation. In order to reduce the computational effort, substitute models are usually constructed to analyze the uncertainty [34]. Deep neural network (DNN) is a deep artificial neural network, which performs high-level abstract processing of data through multi-layer nonlinear mapping. The quantification of uncertain parameters by neural networks has been widely used in model prediction. Using its high-dimensional data processing ability, an improved algorithm combining DNN and UDR is established to study the uncertainty quantification of high-dimensional parameters of EIT forward problem. [35].

Three normalized circular finite element models are established with random uniform conductivity distribution.

In this paper, we studied the high-dimensional uncertainty of the conductivity in the EIT forward problem. Firstly, three normalized circular finite element models with different complexity are established. Then DNN was constructed as an alternative model of EIT. Taking MCS as the benchmark, the output of DNN network model was analyzed by UDR. Finally, evaluate the model from multiple perspectives such as generalization ability, stability, accuracy, and computational efficiency. The results show that DNN-UDR is an efficient and high-precision method, which effectively alleviates the ''curse of dimensionality'' difficulty of existing methods when facing high-dimensional uncertainty problems.

II. THEORY AND METHODS

A. UNCERTAINTY IN EIT FORWARD PROBLEM MODELING

The mathematical model of EIT is given by Maxwell's equations. Since the sufficiently low frequency of the electrical current being applied, the displacement current can be ignored, and only the conductivity should be considered. Given the conductivity σ inside the object, the boundary voltage φ satisfies the Laplace equation

$$\begin{cases} \nabla \cdot \sigma \nabla \varphi = 0 & \text{in } \Omega \\ \varphi = \varphi_0 & \text{in } \Gamma_1 \\ \sigma \dfrac{\partial \varphi}{\partial n} = -J_n & \text{in } \Gamma_2 \end{cases} \tag{1}$$

where, φ_0 is the measured boundary voltage vector, J_n denotes the current intensities on the boundary, and n is the outward normal.

EIT forward problem is to calculate the voltage distribution of the object including the boundary by the given boundary excitation conditions and known object conductivity distribution. It is the basis of inverse problem.The partial differential equation is actually an elliptic equation. For irregular shape domain, there is no analytical solution, so the voltage distribution caused by the inject currents must be calculated by numerical method. Finite element method (FEM) is commonly used because it can fit arbitrary boundary and deal with complex mediums well [36].

B. UNIVARIATE DIMENSION REDUCTION METHOD

UDR is a numerical integration method that can deal with high-dimensional parameter problems, accurately predict statistical moments and reliability. Consider a performance function $\boldsymbol{Y}$ with multi-variables input $\boldsymbol{X}$expressed as follows

$$\boldsymbol{Y} = g(\boldsymbol{X}) \tag{2}$$

where, $\boldsymbol{X} = [X_1, X_2, \cdots, X_d] \in R^d$ is the d-dimensional random input variable whose probability density function (PDF) is $f_{\boldsymbol{X}}(x)$, x is the samples of input variables.

1) DECOMPOSITION OF SINGLE ARGUMENT

The mean value of a univariate is usually taken as the reference point, and $g(\boldsymbol{X})$ can be decomposed at μ_i. Equation (2) can be expressed as

$$\begin{aligned} g(X) \approx \hat{g}(X) &= \hat{g}(X_1, \cdots, X_d) \\ &= \sum_{i=1}^{d} g(\mu_1, \cdots, \mu_{i-1}, X_i, \mu_{i+1}, \cdots, \mu_d) \\ &\quad - (d-1) g(\mu_1, \cdots, \mu_d) \end{aligned} \tag{3}$$

where, $g(\mu_1, \cdots, \mu_{i-1}, X_i, \mu_{i+1}, \cdots, \mu_d)$is a random variable with $X = (\mu_1, \cdots, \mu_{i-1}, X_i, \mu_{i+1}, \cdots, \mu_d)$; $g(\mu_1, \cdots, \mu_d)$is a deterministic response when $X_i = \mu_i$. The right-hand side functions with only one variable is equal to the left-hand side.

2) CALCULATION OF THE r-ORDER STATISTICAL MOMENT

After the decomposition of single argument of $g(\boldsymbol{X})$, the second step of UDR is to solve the r-order statistical moment of $\hat{g}(X)$. That is, directly integrate (3), the r-order statistical moment m_r is

$$m_r \approx E[\hat{g}^r(\boldsymbol{X})] \tag{4}$$

where, $E(\bullet)$ represents the mathematical expectation operator.

The r-order statistical moment of $g(\boldsymbol{X})$ is expanded based on the binomial theorem

$$\begin{aligned} m_r \approx \sum_{i=0}^{r} \binom{r}{i} E\left\{ \left[\sum_{j=1}^{d} g(\mu_1, \cdots, \mu_{j-1}, X_j, \mu_{j+1}, \cdots, \mu_d) \right]^i \right. \\ \left. [-(d-1) g(\mu_1, \cdots, \mu_d)]^{r-i} \right\} \end{aligned} \tag{5}$$

Equation (5) can be expanded based on the binomial theorem and defined as follows. Define

$$S_q^i = E\left\{ \left[\sum_{j=1}^{d} g(\mu_1, \cdots, \mu_{j-1}, X_j, \mu_{j+1}, \cdots, \mu_d) \right]^i \right\} \tag{6}$$

where, $q = 1, \cdots, d, i = 1, \cdots, r$.

Equation (6) can be recursively expanded to

$$S_d^i = \sum_{k=0}^{i} \binom{i}{k} S_{d-1}^k E\left[g^{i-k}(\mu_1, \cdots, \mu_{d-1}, X_d) \right] \tag{7}$$

where, $q = 1, \cdots, d, i = 1, \cdots, r$.

Substitute (7) into (5), the general expression of r-th order statistical moment of $g(\boldsymbol{X})$ can be obtained.

$$m_r \approx \sum_{i=0}^{r} \binom{r}{i} S_d^i [-(d-1) g(\mu_1, \cdots, \mu_d)]^{r-i} \tag{8}$$

In (7) and (8), only one unknown term need to be computed.

$$\begin{aligned} &E\left[g^h(\mu_1, \cdots, \mu_{j-1}, X_j, \mu_{j+1}, \cdots, \mu_d) \right] \\ &= \int g^h(\mu_1, \cdots, \mu_{j-1}, X_j, \mu_{j+1}, \cdots, \mu_d) f_{X_j}(x_j) dx_j \end{aligned} \tag{9}$$

where, $h = i\text{-}k, f_{X_j}(x_j)$ is the marginal probability density of X_j, which can be calculated from the known type of random variables. Therefore, the solution of the r-th order statistical moment of $g(\boldsymbol{X})$ is converted to multi univariate calculations.

3) SOLVING OF MULTI UNIVARIATE INTEGRALS

UDR reduces the calculation of a d-dimensional integral to the calculation of several one-dimensional integrals essentially. From a mathematical point of view, an interpolation integral such as Gaussian interpolation quadrature formula should be applied to solve the higher order integral solution. (9) can be described as

$$\begin{aligned} &E\left[g^h(\mu_1, \cdots, \mu_{j-1}, X_j, \mu_{j+1}, \cdots, \mu_d) \right] \\ &= \int g^h(\mu_1, \cdots, \mu_{j-1}, X_j, \mu_{j+1}, \cdots, \mu_d) f_{X_j}(x_j) dx_j \\ &\approx \sum_{i=1}^{m} \omega_{ji} \left[g(\mu_1, \cdots, \mu_{j-1}, l_{ji}, \mu_{j+1}, \cdots, \mu_d) \right]^h \end{aligned} \tag{10}$$

where, $g(\mu_1, \cdots, \mu_{j-1}, l_{ji}, \cdots, \mu_{j+1}, \mu_d)$ is a one-dimensional random variable function corresponding to the j-th dimension variable.

As mentioned above, it is simpler to change the calculation of one function with d-dimensional variables to the calculation of d functions with one-dimensional variable. The commonly used distribution types of random variables are uniform distribution, normal distribution and exponential distribution. After obtaining the nodes and weights of one-dimensional variables, the r-order statistical moment of $g(\boldsymbol{X})$ in (7) and (5) are solved.

C. THEORY OF DEEP NEURAL NETWORK MODELING

Considering the high nonlinearity, high dimension and sufficient sample size of EIT forward problem, DNN is chosen as the substitute model. The process of modeling a network usually involves the following steps.

1) THE DESIGN OF NETWORK STRUCTURE

In the network structure of EIT forward problem, the input layer x refers to the conductivity distribution with multiple uncertain parameters, and the output layer y is the boundary voltage distribution. The loss function is a measure of the difference between the predicted voltage distribution and actual

value. The smaller the loss function, the better the robustness of the network.

We choose mean square error (MSE) as the loss function, and the network training problem becomes a function minimization problem, that is, minimizing MSE calculated by the predicted voltage value $\hat{u}$ and actual value u.

$$Loss = \frac{1}{N} \min_{(w,b)} \sum_{i=1}^{N} (u_i - \hat{u}_i)^2 \tag{11}$$

where, N is the number of samples and $\hat{u}_i$ is the predicted value on the i-th electrode of the models, w and b refer to the weights and biases value of the network, respectively.

2) THE SELECTION OF OPTIMAL MODEL

DNN is a kind of network containing a large number of hidden layers. Nonlinearity of the neural network is achieved by using an affine transformation followed by an activation function.In deep learning, Leaky_Rectified linear unit (Leaky_ReLU) is generally used as the activation function of intermediate hidden neurons [37]. Leaky_ReLU is defined as

$$y = \begin{cases} x, x \geq 0 \\ \alpha x, x < 0 \end{cases} \tag{12}$$

where α is a small number selected according to experience, and we set $\alpha = \mathbf{0.2}$ in this paper.

3) THE OPTIMIZATION OF NETWORK

The affine transformation is controlled by learned parameters including the weights w and biases b. We use adaptive moments (Adam) method to optimize the parameters, because it can calculate the adaptive learning rate of each parameter and has a fast convergence speed, which avoids the problem of difficult selection of learning rate in gradient descent method [38].

In addition, during the process of network training, with the deepening of the network, the expression ability is enhanced, but the training accuracy is reduced. It's necessary to add the residual structure to the network structure to avoid the network degradation.

III. SIMULATION EXPERIMENT AND RESULTS

A. THE ESTABLISHMENT OF TWO-DIMENSIONAL CIRCLE SIMULATION MODELING

The uncertainty quantification of the conductivity oriented to the EIT requires geometric models. We can build various models with different levels of complexity according to different requirements. For 2D simulation, the circular models are used. For the same object, the finer subdivision, the more elements, the more complex the model, and the higher the resolution of the imaging.

In Fig. 1, three normalized two-dimensional circular models with different elements are established. In EIT modeling, different element has different conductivity parameter. In order to ensure sufficient accuracy, the element number in FEM will be relatively large, which increases the uncertainty

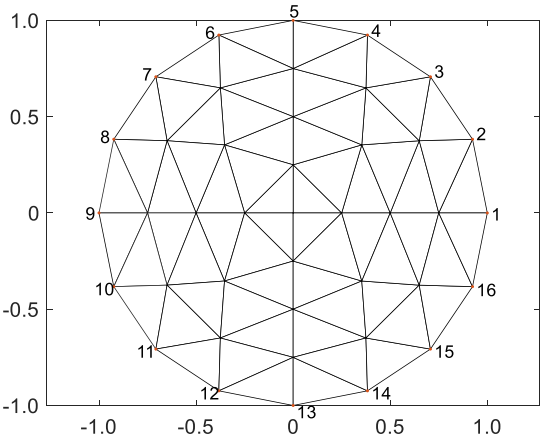

(a) model 1 (d=64)

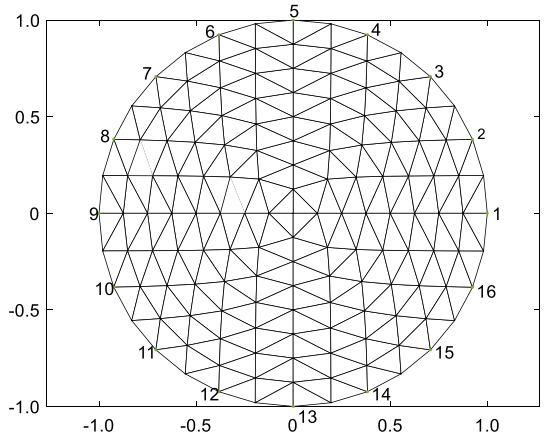

(b) model 2 (d=256)

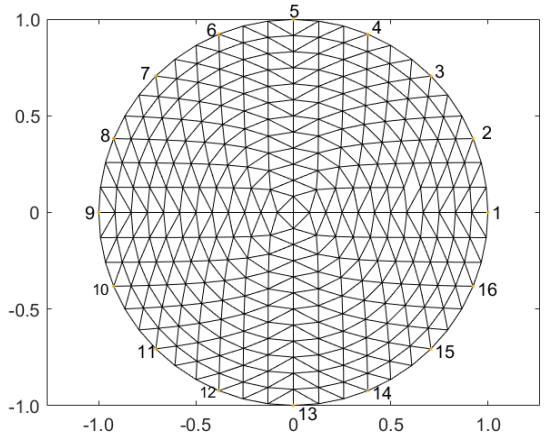

(c) model 3 (d=576)

FIGURE 1. Two-dimensional circular domain subdivision model.

of the model [39]. So the dimensions of variable parameters are **64**, **256** and **576** in three models respectively. In addition, the **16** electrodes are evenly placed on the edge of the unit circle. The excitation current of relative injection is **1 mA**, **50 Hz.**

B. THE SOLUTION OF EIT FORWARD PROBLEM BASED ON DEEP NEURAL NETWORK SUBSTITUTE MODEL

1) THE GENERATION OF DATASET FOR SUBSTITUTE MODELS OF EIT

DNN is chosen as the substitute model to compute EIT forward problem. In Fig. 1, the radius of the outermost scalp of the two-dimensional circular model of EIT is **10 cm**, and **16** electrodes are placed on the scalp surface to excite the current and measure the boundary voltage. In the way of relative current excitation, the **1-9** electrode pair is used to inject current, that is, the inflow of electrode **1** and the outflow of electrode **9**. The excitation current is **1 mA**, and electrode **9** is the reference zero potential. The input random variable of the model is the conductivity value of each element, the output random variable is the boundary voltage value of the two-dimensional circular model, and the uncertainty dimension describing this system is the number of triangular elements in Fig. 1. The conductivity change of each element is assumed to follow a uniform distribution with a mean of **1** and a rate of change of $\pm$**20%**. The input set of the model is the generated **10000** groups of random variables. Then added to the EIT finite element program to obtain the boundary voltage value as output and analyzed by statistical methods.

2) THE STRUCTURE OF DNN NETWORK MODEL

The model consists of **9** layers of fully connected network and residual structure. On the basis of sequential direct connection, the connecting bridge is added every two layers as residual structure. The solver is implemented in the Python library TensorFlow. We generated the dataset of $N \times d$ pairs of voltage and conductivity. The dataset is randomly generated and split into three parts - a set of 8×10^5 training examples, a set of 2×10^5 validation examples and a set of 1×10^5 test examples. We set the Adam optimization learning rate to be 1×10^{-5}. The batch size is set to be **50**. After each training, the learning rate decays to the original **0.80**.

3) THE TEST RESULTS OF DNN NETWORK MODEL

In this paper, model **2** is used to show the evaluation results of the generalization ability of DNN networks.

In Fig. 2, **100** sample points are randomly selected from the newly generated sample set, where the blue dot line is the predicted value and the red dot line is the actual value. The results show that the DNN predicted data output is consistent with the output of the test data set.

For the constructed DNN substitute model, the average absolute percentage error ε is defined to test the accuracy for samples:

$$\varepsilon = \frac{1}{N} \sum_{i=1}^{N} \frac{\left| u_i - \hat{u}_i \right|}{u_i} \tag{13}$$

where, N is the number of test samples, u_i is the calculated value of the EIT, and $\hat{u}_i$ is the predicted value of DNN model. TABLE 2 shows the average absolute percentage error value of each electrode. The value of $(1\text{-}\varepsilon) \times 100\%$ represents the accuracy of the model.

TABLE 1. The structure of DNNs.

model 1	model 2	model 3
Inputs	Inputs	Inputs
FC-64	FC-256	FC-512
FC-128	FC-512	FC-1024
RS-0.7	RS-0.7	RS-0.7
FC-256	FC-1024	FC-2048
FC-128	FC-1024	FC-4096
RS-0.7	RS-0.7	RS-0.7
FC-64	FC-512	FC-2048
	FC-256	FC-1024
		RS-0.7
		FC-512

TABLE 2. Average absolute percentage error of the voltage at the boundary electrode with 256 uncertainties.

Electrode index	ε	Electrode index	ε
1	0.007 6	9	0.012 9
2	0.005 9	10	0.005 3
3	0.002 3	11	0.002 6
4	0.004 7	12	0.001 0
5	0.009 7	13	0.005 8
6	0.001 2	14	0.003 2
7	0.004 1	15	0.013 5
8	0.000 2	16	0.020 2

It can be seen from TABLE 2 Furthermore, the other two FEM models obtain the similar results with model **2**. Therefore, DNN can be used as an effective substitute model to calculate EIT forward problems.

In addition, considering the similarity of the model experiment process and the length of the paper, we leave the test results and codes of other models to the interested reader to look up. These data are publicly available and the websites are listed in the Appendix

C. THE UNCERTAINTY SOLUTION OF EIT FORWARD PROBLEM BASED ON DNN-UDR

Taking model **2** as the example, we assume that the conductivity parameters follow a random uniform distribution in the range of **0.8-1.2 S/m**. The DNN is used as substitute model, and the UDR is applied to quantify the uncertainty of voltage in the EIT forward problem.

Combining (3) and (10), the mean conductivity points are selected as a set of reference points, the sample number is 1×10^5. The PDF distribution, mean value of output voltage,

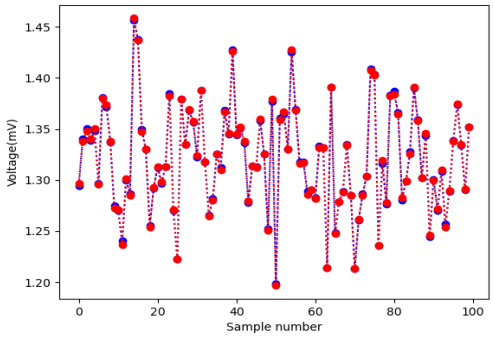

(a) electrode 1

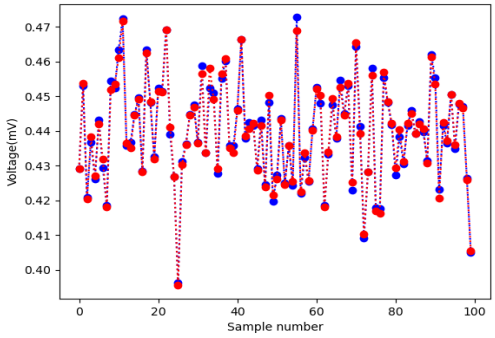

(b) electrode 3

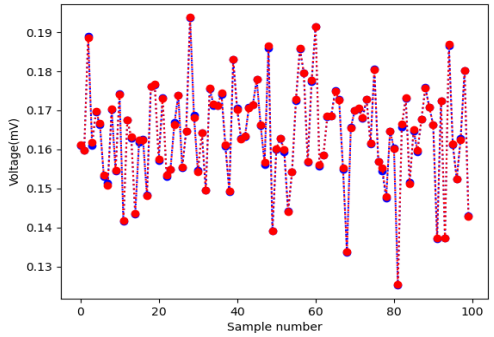

(c) electrode 5

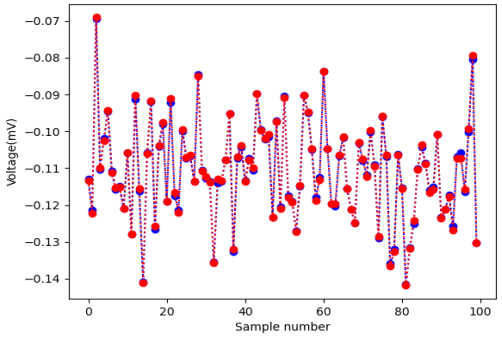

(d) electrode 7

FIGURE 2. DNN generalization ability test diagram of some electrodes.

and other voltage statistics are estimated from DNN-UDR predictions.

Some quantification parameters such as mean value, standard deviation, the average absolute percentage error, variation coefficient and covariance are used to compare the performance of UDR and MCS, as shown in Fig. 4 - Fig. 7.

1) PROBABILITY DENSITY FUNCTION DISTRIBUTION

Fig. 3 shows a PDF diagram of partial electrode voltages, where the x-coordinates represent the voltage values.

It can be seen from Fig. 3 that DNN-UDR and MCS fit well. Their PDF distribution trend is basically the same. The PDF calculated by DNN-UDR fits MCS and consistent with the prediction results of DNN.

2) MEAN VALUE

The mean value is used to quantify UQ accuracy as illustration in Fig. 4, where the x-coordinates represent the boundary electrode indexes, and the y-coordinates are the corresponding mean voltage values.

In Fig. 4, the mean value of the voltage distribution gets maximum at the injection electrode. It decreases with the increase of the distance from the injection to output electrode, and reaches the minimum at the output electrode. The curve trend is accordance with the objective situation, and the DNN-UDR results fit well with the MCS.

3) STANDARD DEVIATION

The standard deviation is used to describe the deviation degree of random variable distribution X relative to its mean value. The results are illustrated in Fig. 5, where the x-coordinates represent the boundary electrode indexes, and the y-coordinates are the corresponding standard deviation values.

It can be seen from Fig. 5 that the DNN-UDR results are consistent with the MCS results. Furthermore, comparing with the standard deviation values in different models, the standard deviation gradually decreases with the increase of subdivision size. For each subsection size, the standard deviation of the excitation points is the largest, indicating that the change of conductivity has the greatest influence on the excitation points.

4) VARIATION COEFFICIENT

The variation coefficient η is used to measure the dispersion degree of the predicted value, which represents the stability of the model. The calculation formula is

$$\eta = \left| \frac{\mu}{Var} \right| \tag{14}$$

where, μ is the mean value of sample, Var is the sample variance. The quantization standard of the variation coefficient is shown in TABLE 3. The results are illustrated in Fig. 6, where the x-coordinates represent the boundary electrode indexes, and the y-coordinates are the corresponding variation coefficient values.

Fig. 6 shows that the results obtained by the two methods in the three models are consistent, and with the increase

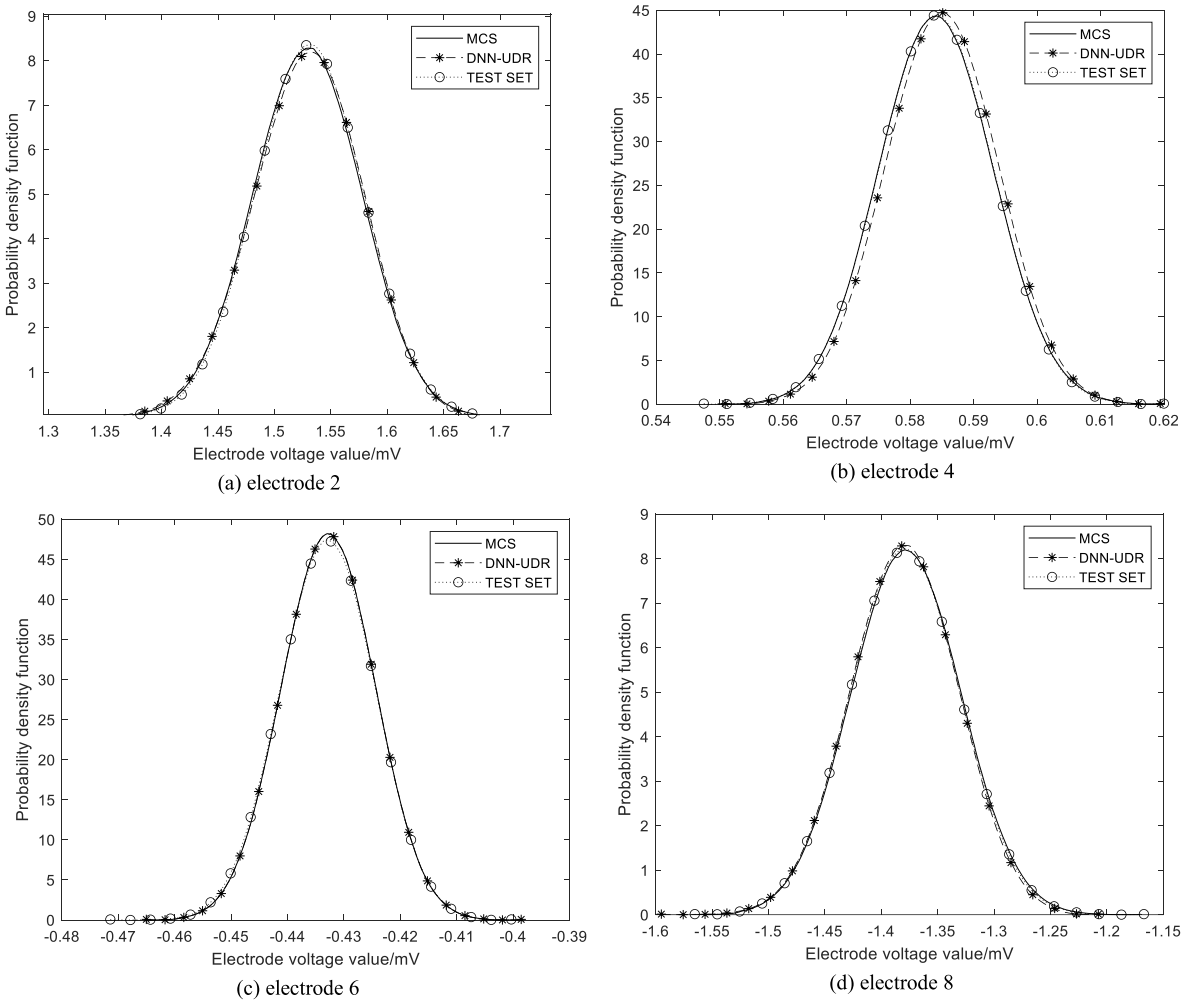

FIGURE 3. Probability density distribution of voltages in a two-dimensional circle model with 256.

TABLE 3. Model stability quantization table.

η	The stability of the model structure
≤0.2	The fluctuations are very small, very stable
≤0.4	Small fluctuation, basically stable
≤0.6	General fluctuation, not very stable
≤0.8	Large fluctuations, not very stable
>0.8	High variation, great randomness

dimensions of variable parameters, the variation coefficient value becomes smaller and smaller, and the model tends to be stable.

5) AVERAGE ABSOLUTE PERCENTAGE ERROR

We use the average absolute percentage error defined in (13) to determine the accuracy of model prediction. The comparison results between DNN-UDR and MCS are shown in Fig. 7.

In Fig. 7, the results consistent well with the variation coefficient. The influence of the conductivity on the model prediction decreases gradually, and the accuracy of the model predicted value increases.

TABLE 4. Mean and covariance of the voltage at the boundary electrode.

Electrode index	Methods	Mean	COV
2	MCS	0.584 2	0.000 06
	DNN-UDR	0.584 9	0.000 06
8	MCS	0.433 0	0.000 06
	DNN-UDR	0.433 3	0.000 06
9	MCS	1.378 0	0.001 82
	DNN-UDR	1.380 0	0.001 78
10	MCS	0.433 0	0.000 05
	DNN-UDR	0.432 7	0.000 05

6) COVARIANCE

To describe the relationship between variables, covariance (COV) can be calculated as

$$COV = \frac{\sum_{i=1}^{N}(X_i - \bar{X})(Y_i - \bar{Y})}{N-1} \tag{15}$$

where, $\bar{X}$ is the mean values of variables $\boldsymbol{X}$ and $\bar{Y}$ is the mean values of variables $\boldsymbol{Y}$, and N is the number of samples. The

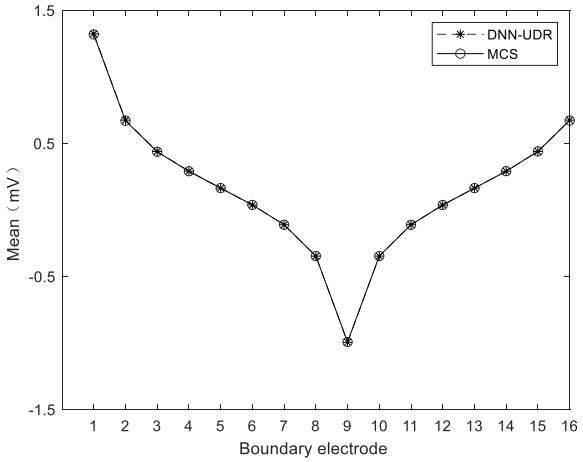

(a) d=64

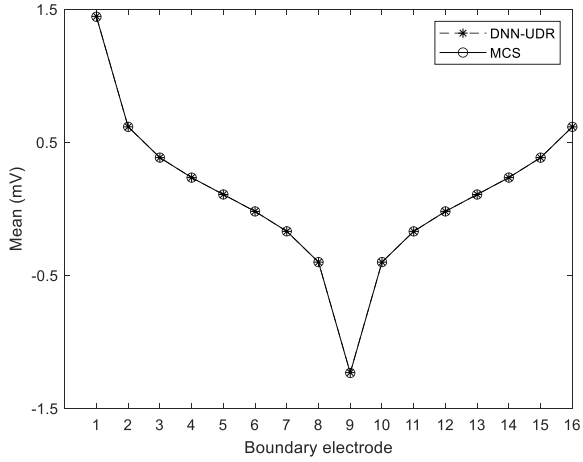

(b) d=256

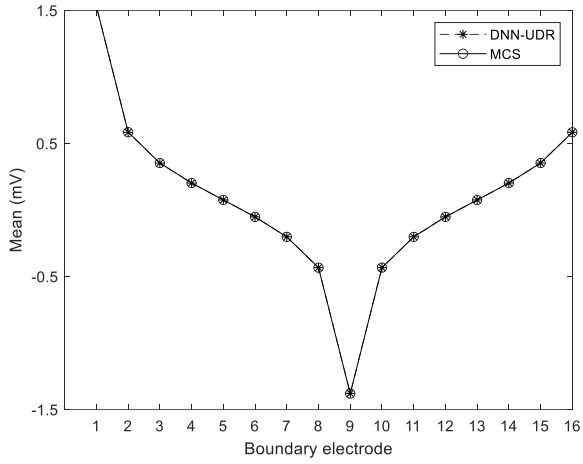

(c) d=576

FIGURE 4. Mean values of boundary electrode voltage for different number of uncertain parameters.

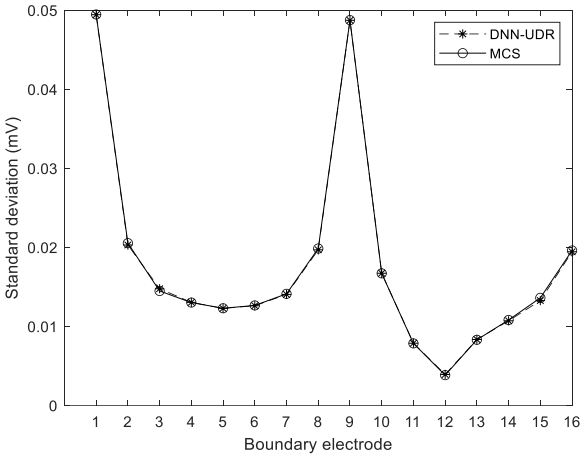

(a) d=64

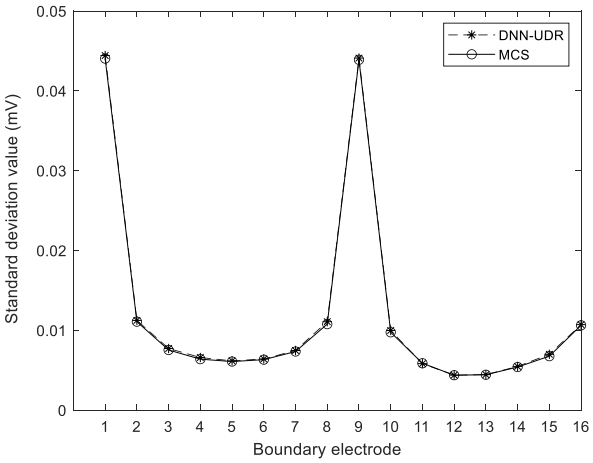

(b) d=256

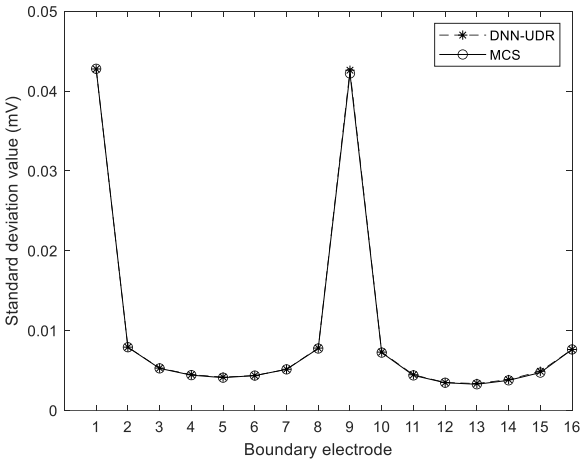

(c) d=576

FIGURE 5. Standard deviation of boundary electrode voltage for different number of uncertain parameters.

mean value and covariance on different boundary electrodes are shown in TABLE 4.

It can be seen from TABLE 4, the interaction between the variables is small, and the boundary electrode voltage values calculated by the two UQ methods fit well.

7) COMPUTING EFFICIENCY

Computational efficiency is also an important factor to measure the simulation methods. The simulations have been run on a Windows machine equipped with X64 processor

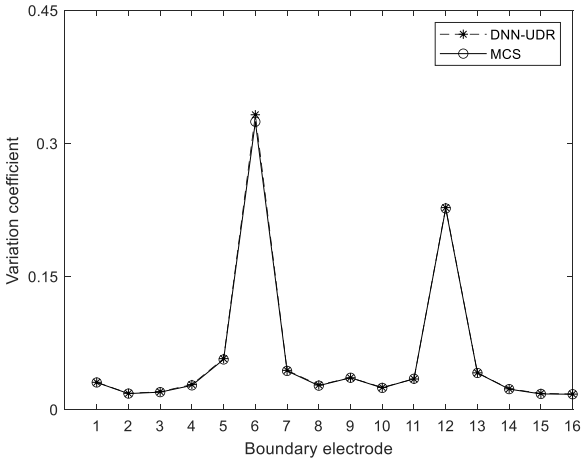

(a) d=64

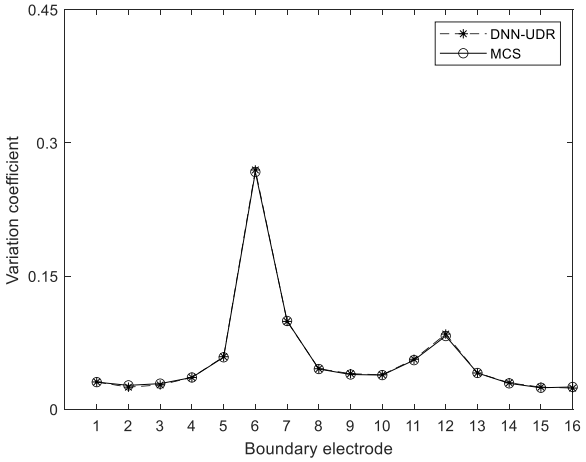

(b) d=256

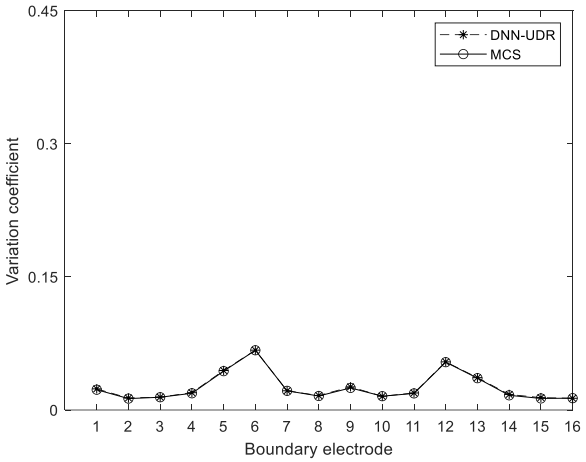

(c) d=576

FIGURE 6. Variation coefficients of boundary electrode voltage for different number of uncertain parameters.

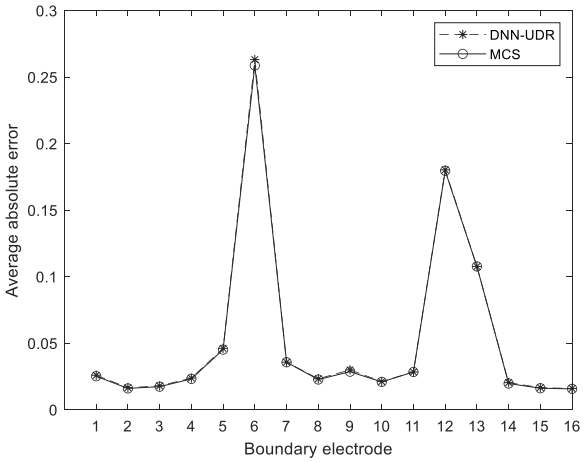

(a) d=64

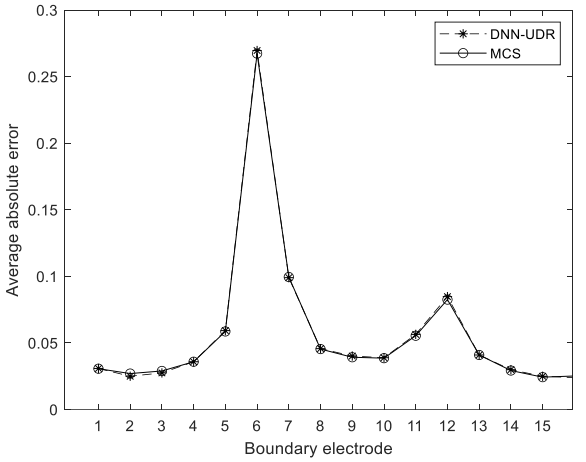

(b) d=256

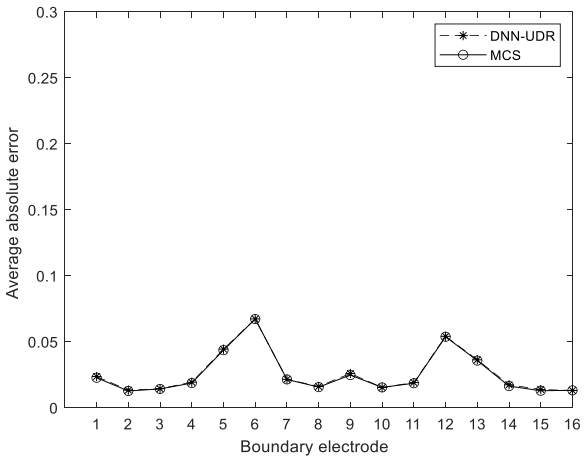

(c) d=576

FIGURE 7. Average absolute error of boundary electrode voltage for different number of uncertain parameters.

(Intel(R) Core(TM) i5-9300H CPU @ 2.40GHz). The results are executed in MATLAB 2019 and Python 3.6. The calculation time results are shown in TABLE 5.

It can be seen from TABLE 5 that with the increase of uncertain parameter d, the calculation time of MCS increases significantly, while DNN-UDR changes little. In addition, DNN-UDR saves two orders of magnitude in calculation time with MCS.

TABLE 5. Calculation time for different number of uncertain parameters.

Methods	calculation time /(s)		
	d=64	d=256	d=576
DNN-UDR	8.32	9.74	9.87
MCS	721.39	9 256.88	10 942.84

IV. CONCLUSION

In this paper, DNN-UDR has been proposed for the uncertainty solution of EIT forward problem. Taking the traditional MCS method as benchmark, three normalized FEM circle models with uncertainty number of **64**, **256**, **576** are established with uniform conductivity distribution.

Firstly, DNN is used as a substitute model for finite element calculation of EIT forward problem and the results show its strong generalization ability and good robustness. Then, based on the DNN substitute model, UDR is used to quantify the uncertainty. The probability density function and the quantification parameters of DNN-UDR are consistent with MCS, indicating that the results are reliable. The comparison with three simulation models show that with the increase of the parameter dimension, the stability of the model becomes more and more better, and the advantages of DNN-UDR in computational efficiency become more obvious. In a word, the results show that DNN-UDR can effectively solve the difficulty of ''curse of dimensionality''. It is of great significance to improve the quality of reconstructed images.

Furthermore, our study provides a reference for high-dimensional uncertainty quantification problem, and also hopeful for the quantitative study of other structural uncertainties.

APPENDIX
REPLICATION OF RESULTS

Considering the similarity of the model experiment process and the length of the paper, we put the test results and codes of other models on a public website. All the experiments and codes related to this paper that can be found in the web site https://github.com/eit-uq/code

ACKNOWLEDGMENT

The authors would like to thank all the authors for their contributions. The authors have no conflicts of interest relating to the content of this article.

REFERENCES

[1] Z. Xu, J. Yao, Z. Wang, Y. Liu, H. Wang, B. Chen, and H. Wu, ''Development of a portable electrical impedance tomography system for biomedical applications,'' *IEEE Sensors J.*, vol. 18, no. 19, pp. 8117–8124, Oct. 2018.

[2] H. Dai, G. J. Gallo, T. Schumacher, and E. T. Thostenson, ''A novel methodology for spatial damage detection and imaging using a distributed carbon nanotube-based composite sensor combined with electrical impedance tomography,'' *J. Nondestruct. Eval.*, vol. 35, no. 2, pp. 26–35, Jun. 2016.

[3] D. Smyl, R. Rashetnia, A. Seppänen, and M. Pour-Ghaz, ''Can electrical resistance tomography be used for imaging unsaturated moisture flow in cement-based materials with discrete cracks?'' *Cement Concrete Res.*, vol. 91, pp. 61–72, Jan. 2017.

[4] T. Rymarczyk, J. Sikora, P. Adamkiewicz, K. Niderla, and P. Tchórzewski, ''Analysis and monitoring of flood embankments through image reconstruction based on electrical impedance tomography,'' in *Proc. 19th Int. Symp. Electromagn. Fields Mechtron., Electr. Electron. Eng. (ISEF)*, Aug. 2019, pp. 1–2.

[5] V. Chitturi and N. Farrukh, ''Spatial resolution in electrical impedance tomography: A topical review,'' *J. Electr. Bioimpedance*, vol. 8, no. 1, pp. 66–78, Jul. 2017.

[6] A. Adler and A. Boyle, ''Electrical impedance tomography: Tissue properties to image measures,'' *IEEE Trans. Biomed. Eng.*, vol. 64, no. 11, pp. 2494–2504, Nov. 2017.

[7] Y. Kuwahara, A. Nozaki, and K. Fujii, ''Large scale analysis of complex permittivity of breast cancer in microwave band,'' *Adv. Breast Cancer Res.*, vol. 9, no. 4, pp. 101–109, 2020.

[8] D. D. Yero, F. G. González, D. Van Troyen, and G. A. E. Vandenbosch, ''Dielectric properties of ex vivo porcine liver tissue characterized at frequencies between 5 and 500 kHz when heated at different rates,'' *IEEE Trans. Biomed. Eng.*, vol. 65, no. 11, pp. 2560–2568, Nov. 2018.

[9] U. Zurbuchen, F. Poch, O. Gemeinhardt, M. E. Kreis, S. M. Niehues, J. L. Vahldieck, and K. S. Lehmann, ''Determination of the electrical conductivity of human liver metastases: Impact on therapy planning in the radiofrequency ablation of liver tumors,'' *Acta Radiologica*, vol. 58, no. 2, pp. 164–169, Feb. 2017.

[10] C. Tang, F. You, G. Cheng, D. Gao, F. Fu, G. Yang, and X. Dong, ''Correlation between structure and resistivity variations of the live human skull,'' *IEEE Trans. Biomed. Eng.*, vol. 55, no. 9, pp. 2286–2292, Sep. 2008.

[11] S. Suksawang, K. Niamsri, and T. Ouypornkochagorn, ''Scalp voltage response to conductivity changes in the brain in the application of electrical impedance tomography (EIT),'' in *Proc. 15th Int. Conf. Electr. Eng./Electron., Comput., Telecommun. Inf. Technol. (ECTI-CON)*, Chiang Rai, Thailand, Jul. 2018, pp. 223–236.

[12] T. Ouypornkochagorn, ''Constrained modeling for image reconstruction in the application of electrical impedance tomography to the head,'' in *Proc. IEEE 14th Int. Symp. Biomed. Imag. (ISBI)*, Apr. 2017, pp. 548–551.

[13] G. Hacken, ''Uncertainty quantification: Theory, implementation, and applications,'' *Comput. Rev.*, vol. 57, no. 8, pp. 463–464, Dec. 2016.

[14] J. Wang and X. Zheng, ''Review of geometric uncertainty quantification in gas turbines,'' *J. Eng. Gas Turbines Power*, vol. 142, no. 7, pp. 070801–070816, Jun. 2020.

[15] M. Abdar, F. Pourpanah, S. Hussain, D. Rezazadegan, L. Liu, M. Ghavamzadeh, P. Fieguth, X. Cao, A. Khosravi, U. R. Acharya, V. Makarenkov, and S. Nahavandi, ''A review of uncertainty quantification in deep learning: Techniques, applications and challenges,'' *Inf. Fusion*, vol. 76, pp. 243–297, Dec. 2021.

[16] Y. Chen and W. Ma, ''Uncertainty quantification for TRACE simulation of FIX-II No. 5052 test,'' *Ann. Nucl. Energy*, vol. 143, no. 1, pp. 107490–107499, Aug. 2020.

[17] B. S. Guilherme, A. Thielscher, K. H. Madsen, T. R. Knösche, and K. Weise, ''A principled approach to conductivity uncertainty analysis in electric field calculations,'' *NeuroImage*, vol. 188, no. 1, pp. 1–35, Mar. 2019.

[18] X. Zhang, H. Xiao, T. Gomez, and O. Coutier-Delgosha, ''Evaluation of ensemble methods for quantifying uncertainties in steady-state CFD applications with small ensemble sizes,'' *Comput. Fluids*, vol. 203, no. 1, pp. 104530–104565, May 2020.

[19] X. Cheng and V. Monebhurrun, ''Application of different methods to quantify uncertainty in specific absorption rate calculation using a CAD-based mobile phone model,'' *IEEE Trans. Electromagn. Compat.*, vol. 59, no. 1, pp. 14–23, Feb. 2017, doi: 10.1109/TEMC.2016.2605127.

[20] T. Hou, D. Nuyens, S. Roels, and H. Janssen, ''Quasi-Monte Carlo based uncertainty analysis: Sampling efficiency and error estimation in engineering applications,'' *Rel. Eng. Syst. Saf.*, vol. 191, Nov. 2019, Art. no. 106549.

[21] A. Abdedou and A. Soulaimani, ''A non-intrusive B-splines Bézier elements-based method for uncertainty propagation,'' *Comput. Method Appl. Mech. Eng.*, vol. 345, no. 1, pp. 774–804, Mar. 2019.

[22] P. Ni, Y. Xia, J. Li, and H. Hao, ''Using polynomial chaos expansion for uncertainty and sensitivity analysis of bridge structures,'' *Mech. Syst. Signal Process.*, vol. 119, pp. 293–311, Mar. 2019.

[23] H.-P. Wan, W.-X. Ren, and M. D. Todd, ''Arbitrary polynomial chaos expansion method for uncertainty quantification and global sensitivity analysis in structural dynamics,'' *Mech. Syst. Signal Process.*, vol. 142, Aug. 2020, Art. no. 106732.

[24] S. H. Lee and W. Chen, "A comparative study of uncertainty propagation methods for black-box-type problems," *Structural Multidisciplinary Optim.*, vol. 37, no. 3, pp. 239–253, Jan. 2009.
[25] K. Weise, L. D. Rienzo, H. Brauer, J. Haueisen, and H. Toepfer, "Uncertainty analysis in transcranial magnetic stimulation using nonintrusive polynomial chaos expansion," *IEEE Trans. Magn.*, vol. 51, no. 7, pp. 1–8, Jul. 2015.
[26] A. Gray, S. Ferson, O. Kosheleva, and V. Kreinovich, "While, in general, uncertainty quantification (UQ) is NP-hard, many practical UQ problems can be made feasible," in *Proc. IEEE Symp. Ser. Comput. Intell. (SSCI)*, Dec. 2021, pp. 1–6.
[27] G. Feng, L. Liu, W. Cui, and F. Wang, "Electron beam irradiation on novel coronavirus (COVID-19): A Monte–Carlo simulation," *Chin. Phys. B*, vol. 29, no. 4, Apr. 2020, Art. no. 048703.
[28] Z. Fei, Y. Huang, J. Zhou, and Q. Xu, "Uncertainty quantification of crosstalk using stochastic reduced order models," *IEEE Trans. Electromagn. Compat.*, vol. 59, no. 1, pp. 228–239, Feb. 2017.
[29] F. Xiong, S. Greene, W. Chen, Y. Xiong, and S. Yang, "A new sparse grid based method for uncertainty propagation," *Structural Multidisciplinary Optim.*, vol. 41, no. 3, pp. 335–349, Apr. 2010.
[30] S. Rahman and H. Xu, "A univariate dimension-reduction method for multi-dimensional integration in stochastic mechanics," *Probabilistic Eng. Mech.*, vol. 19, no. 4, pp. 393–408, Oct. 2004.
[31] H. Xu and S. Rahman, "A generalized dimension-reduction method for multidimensional integration in stochastic mechanics," *Int. J. Numer. Methods Eng.*, vol. 61, no. 12, pp. 1992–2019, Nov. 2004.
[32] R. Torchio, L. Di Rienzo, and L. Codecasa, "Stochastic PEEC method based on polynomial chaos expansion," *IEEE Trans. Magn.*, vol. 55, no. 6, pp. 1–4, Jun. 2019.
[33] H. Xu and S. Rahman, "Decomposition methods for structural reliability analysis," *Probabilistic Eng. Mech.*, vol. 20, no. 3, pp. 239–250, Jul. 2005.
[34] S. Tennøe, G. Halnes, and G. T. Einevoll, "Uncertainpy: A Python toolbox for uncertainty quantification and sensitivity analysis in computational neuroscience," *Frontiers Neuroinform.*, vol. 12, p. 49, Aug. 2018.
[35] Z. Wei, D. Liu, and X. Chen, "Dominant-current deep learning scheme for electrical impedance tomography," *IEEE Trans. Biomed. Eng.*, vol. 66, no. 9, pp. 2546–2555, Sep. 2019.
[36] N. Huang, Y. Ma, M. Zhang, H. Ge, and H. Wu, "Finite element modeling of human thorax based on MRI images for EIT image reconstruction," *J. Shanghai Jiaotong Univ. Sci.*, vol. 26, no. 1, pp. 33–39, Feb. 2021.
[37] X. Glorot, A. Bordes, and Y. Bengio, "Deep sparse rectifier neural networks," in *Proc. 14th Int. Conf. Artif. Intell. Statist.*, Jun. 2011, pp. 315–323.
[38] B. Nguyen, C. Morell, and B. De Baets, "Scalable large-margin distance metric learning using stochastic gradient descent," *IEEE Trans. Cybern.*, vol. 50, no. 3, pp. 1072–1083, Mar. 2020.
[39] X. Zhang, G. Xu, S. Zhang, Y. Li, Y. Guo, Y. Li, Y. Wang, and W. Yan, "A numerical computation forward problem model of electrical impedance tomography based on generalized finite element method," *IEEE Trans. Magn.*, vol. 50, no. 2, pp. 1045–1048, Feb. 2014.

YINGGE ZHAO was born in Xuchang, Henan, China. She received the B.S. degree in biomedical engineering from Nanchang Hangkong University, in 2018, and the M.S. degree in biomedical engineering from the Hebei University of Technology, in 2021.

Her research interests include biomedical electromagnetic technology and neural engineering. She is in charge of one scientific and artificial intelligence in Henan Province and participated in the completion of one Natural Science Foundation Project in Hebei Province.

LINGYUE WANG was born in Tangshan, Hebei, China. He received the B.S. degree from the University of Electronic Science and Technology, China, in 2016. He is currently pursuing the Ph.D. degree in electrical engineering with the Hebei University of Technology. He has participated in a number of national, provincial and ministerial research projects, and engaged in the research of biomedical electromagnetic technology and neural engineering, and has made remarkable achievements.

YING LI was born in Dongping, Shandong, China. She received the M.S. and Ph.D. degrees from the Hebei University of Technology, in 2000 and 2003, respectively.

Since 1994, she has been with the Hebei University of Technology, where she has been a Professor with the School of Life Science and Health Engineering. She is a doctoral supervisor. She is also a Senior Member of the Chinese Society of Biomedical Engineering. She is the author of three books and more than 50 articles. She obtained the second and third prize of Natural Science of Hebei Province, and presided over the completion of one project of the National Natural Science Foundation of China and three projects of the Hebei Natural Science Foundation of China. She has participated in the research of more than ten national and provincial projects. Her research interests include biomedical electromagnetic technology and neural engineering.

RENJIE HE received the B.S. degree in electronic engineering from Chongqing University, Chongqing, China, in 1984, the M.S. degree in electrical engineering from The 54th Research Institute of CETC, Hebei, China, in 1989, and the Ph.D. degree in biomedical engineering from Tsinghua University, Beijing. He is a highly accomplished data scientist with extensive experience in MRI pulse sequence programming, medical image analysis, data science, numerical methods applications, physiological/pathological modeling and simulation, AI (machine/deep learning) developments and applications, and imaging informatics platform development in China, in 1998. Currently, he is a Data Scientist in radiation oncology with the MD Anderson Cancer Center, TX, USA, where he specializes in MRI for radiation oncology studies and high performance computation. Additionally, he has extensive experience in developing imaging informatics platforms, such as XNAT and NIBC.

CHONGLEI MA was born in Zhumadian, Henan, China, in 1997. She received the B.S. degree in electrical engineering from the North China University of Water Resources and Electric Power, in 2019, and the M.S. degree in electrical engineering from the Hebei University of Technology, China, in 2023.